Inorganic Chemistry
Cite This: Inorg. Chem. XXXX, XXX, XXX−XXX
Article
pubs.acs.org/IC

Synthesis, Structure, and Physical Properties of the Polar Magnet $DyCrWO_6$

Somnath Ghara,[†] Francois Fauth,[‡] Emmanuelle Suard,[§] Juan Rodriquez-Carvajal,[§] and A. Sundaresan*[,†]

[†]Chemistry and Physics of Materials Unit and School of Advanced Materials, Jawaharlal Nehru Centre for Advanced Scientific Research, Jakkur P.O, 560 064 Bangalore, India

[§]Construction, Equipping and Exploitation of the Synchrotron Light Source (CELLS), ALBA Synchrotron, BP 1413, 08290 Cerdanyola del Vallès, Barcelona, Spain

[‡]Institut Laue Langevin (ILL), 71 Avenue des Martyrs, CS 20156, 38042 Grenoble Cedex 9, France

Supporting Information

ABSTRACT: It has recently been reported that the ordered aeschynite-type polar ($Pna2_1$) magnets $RFeWO_6$ (R = Eu, Tb, Dy, Y) exhibit type II multiferroic properties below T_N ∼ 15−18 K. Herein, we report a comprehensive investigation of the isostructural oxide $DyCrWO_6$ and compare the results with those of $DyFeWO_6$. The cation-ordered oxide $DyCrWO_6$ crystallizes in the same polar orthorhombic structure and undergoes antiferromagnetic ordering at T_N = 25 K. Contrary to $DyFeWO_6$, only a very weak dielectric anomaly and magnetodielectric effects are observed at the Néel temperature and, more importantly, there is no induced polarization at T_N. Furthermore, analysis of the low-temperature neutron diffraction data reveals a collinear arrangement of Cr spins but a noncollinear Dy-spin configuration due to single-ion anisotropy. We suggest that the collinear arrangement of Cr spins may be responsible for the absence of electric polarization in $DyCrWO_6$. A temperature-induced magnetization reversal and magnetocaloric effects are observed at low temperatures.

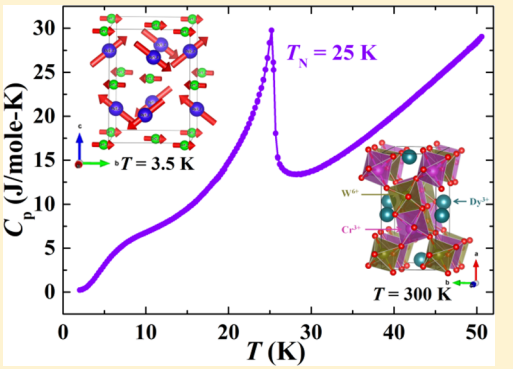

I. INTRODUCTION

Multiferroics are one of the important classes of materials having potential for spintronic devices. However, their direct application is not yet realized because most of the multiferroics discovered so far have low transition temperatures and exhibit a weak magnetoelectric coupling. Therefore, finding new magnetoelectric multiferroics and understanding the mechanism responsible for the magnetoelectric properties are important. Most of the type II multiferroics are centrosymmetric in the paramagnetic state. Spontaneous polarization appears only at the magnetic ordering temperature where certain types of magnetic structures break the spatial inversion symmetry. Typical magnetic structures are the up−up−down−down arrangement of Co^{2+} and Mn^{4+} spins in Ca_3CoMnO_6, the cycloidal magnetic ordering of Mn^{3+} spins in $TbMnO_3$, the transverse conical structure of Cr^{3+} spins in $CoCr_2O_4$, etc.[1−4] All of these materials exhibit strong magnetoelectric coupling because of the common origin of ferroelectric polarization and magnetization. Recently, a few materials, such as Ni_3TeO_6, $M_2Mo_3O_8$ (M = Fe, Mn), $CaBaCo_4O_7$ etc., which are already polar in the paramagnetic region, have been found to be magnetoelectrics (and/or multiferroics) with very strong coupling between the electric and magnetic order parameters below the magnetic ordering temperatures.[5−9] This could be due to the direct involvement of the magnetic ions and their coordinated O ions in making the crystal structure noncentrosymmetric. Such polar magnets exhibiting magnetoelectricity and/or multiferroicity open up a new ground for exploring new magnetoelectric and multiferroic materials with higher Curie temperatures.

Recently, the polar oxides $RFeWO_6$ (R = Dy, Eu, Tb, Y) have been demonstrated to exhibit magnetoelectric multiferroic properties below the magnetic ordering temperature (Néel temperature T_N ∼ 15−18 K) of Fe^{3+} ($3d^5$) ions.[10] Although the polar space group $Pna2_11'$ allows electric polarization along the z direction, no ferroelectric polarization was observed in the paramagnetic state. However, all of these oxides undergo an antiferromagnetic ordering around T_N ∼ 15−18 K, which is associated with an anomaly in the dielectric constant and the appearance of switchable electric polarization. A detailed neutron diffraction study on $DyFeWO_6$ revealed that the magnetic structure of this oxide is characterized by a noncollinear arrangement of both Fe^{3+} and Dy^{3+} spins with a wave vector $\mathbf{k}$ = (0, $^1/_2$, $^1/_2$). The magnetic space group C_ac

Received: July 19, 2018

DOI: 10.1021/acs.inorgchem.8b02023
Inorg. Chem. XXXX, XXX, XXX−XXX

(magnetic point group $m1'$) allows additional polarization along P_x in the magnetically ordered state.[10]

Motivated by these results on $RFeWO_6$, we have investigated an isostructural compound containing Cr^{3+} ($3d^3$) ions, namely, $DyCrWO_6$, using synchrotron X-ray and neutron diffraction experiments, magnetization, heat capacity, and electrical measurements. Our study confirms that this oxide indeed crystallizes in the polar structure (space group $Pna2_1$), similar to the Fe analogue compounds and the recently reported $YCrWO_6$.[10−12] The Cr moments in this compound undergo antiferromagnetic ordering at $T_N \sim 25$ K. In contrast to the Fe counterpart, the Cr compound shows only a weak dielectric anomaly and exhibits no induced polarization at T_N. Furthermore, the magnetic peaks can be indexed with a different wave vector, $\mathbf{k} = (0, 0, 0)$, with quasi-collinear Cr spins but noncollinear Dy spins, as observed in $DyFeWO_6$.

II. EXPERIMENTAL SECTION

A polycrystalline sample of $DyCrWO_6$ was prepared by a conventional solid-state reaction method. Stoichiometric amounts of Dy_2O_3 (preheated at 900 °C for 12 h in air), Cr_2O_3, and WO_3 were mixed, ground, and heated at a final temperature of 1140 °C for 12 h in air with intermittent grindings. Synchrotron X-ray diffraction data were recorded at room temperature at the Materials Science Powder Diffraction beamline (BL04-MSPD) at ALBA Synchrotron (Barcelona, Spain) using a wavelength of $\lambda = 0.3171$ Å.[13,14] Neutron powder diffraction data were collected at several temperatures with the D2B and D1B diffractometers at the ILL, Grenoble, France, using wavelengths of $\lambda = 1.594$ and 2.528 Å, respectively. Magnetization measurements were performed with a Magnetic Property Measurement System (MPMS-SQUID, Quantum Design, Inc., San Diego, CA). The heat capacity was measured with a Physical Property Measurement System (PPMS, Quantum Design, Inc.). The dielectric constant was measured with a LCR meter (Agilent E4980A). Pyroelectric current measurements were performed with an electrometer (Keithley 6517A). All of the electrical measurements were performed in the PPMS.

III. RESULTS AND DISCUSSION

A combined Rietveld refinement of room temperature neutron and synchrotron X-ray diffraction data of $DyCrWO_6$ was performed with the orthorhombic space group $Pna2_1$ using *FullProf* software.[15] Two extra tiny peaks were observed in the synchrotron X-ray diffraction pattern, in addition to the peaks of TiO_2 (from the sample environment used in synchrotron X-ray diffraction experiments); however, we could not identify the impurity phase because of their low intensity. These peaks were excluded in the refinement. The results of the combined Rietveld refinement are shown in Figure 1a,b, and the crystal structure is shown in Figure 2a. The complete structural parameters obtained from the refinement are tabulated in Table 1. Similar to the ordered arrangement of the Fe^{3+} and W^{6+} ions in $DyFeWO_6$, the Cr^{3+} and W^{6+} ions are found to be ordered due to the large differences in their ionic radii and charges, and the CrO_6 and WO_6 octahedra are connected through sharing of their corners and edges. In Figure 2b, a dimer formed by two edge-shared octahedra is shown, where the Cr^{3+}−O and W^{6+}−O bond distances are also given. We tried to prepare the compounds $RCrWO_6$ with other rare-earth elements, but we could not obtain a pure phase using the preparation method followed in this work. The lower stability of these phases could be due to the presence of the edge-shared octahedra of cations with high charges.

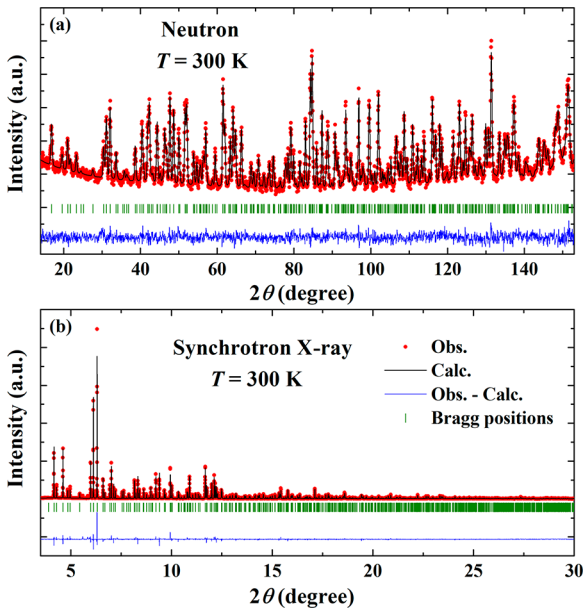

Figure 1. Results of a combined Rietveld refinement of (a) neutron and (b) synchrotron X-ray diffraction data collected at room temperature.

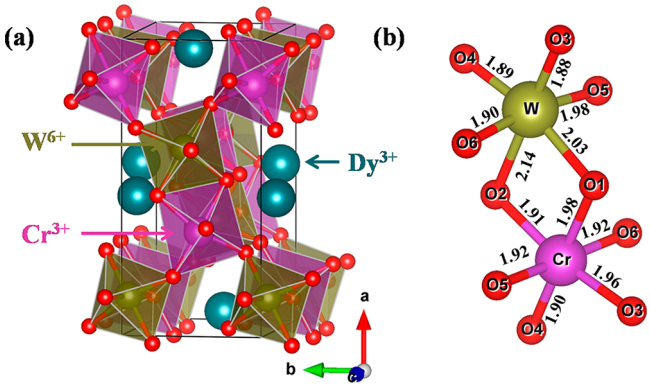

Figure 2. (a) Ordered aeschynite-type crystal structure of $DyCrWO_6$. (b) Edge-shared Cr^{3+} and W^{6+} octahedra showing the bond lengths (in Å).

Figure 3a shows the temperature dependence of the field-cooled (FC) susceptibility $\chi(T)$ measured under a magnetic field of 100 Oe, where the sample was cooled to the lowest temperature in the presence of a magnetic field and the magnetization was measured during warming in the presence of a magnetic field. A clear anomaly is observed around 25 K (T_N) in $\chi(T)$, where a sharp λ-type peak is found in the heat capacity $C_P(T)$ data (inset of Figure 3a), suggesting a long-range magnetic ordering of Cr^{3+} moments. T_N of this compound is slightly higher than those of $RFeWO_6$ compounds. As indicated by analysis of the neutron data (Table S1), the Dy^{3+} moments are induced to order at $T_N = 25$ K, similar to that observed in $DyFeWO_6$.[10] The broad hump observed in the $C_P(T)$ data around 7 K could be a Schottky-type anomaly due to population of the crystal-field levels of Dy^{3+} ions that change with the temperature. The high-temperature magnetization data are fitted with the Curie−Weiss law (shown in Figure S1). The effective paramagnetic moment obtained from the fit is $\mu_{exp} = 11.4\ \mu_B$/formula unit (fu), which is close to the expected effective paramagnetic

DOI: 10.1021/acs.inorgchem.8b02023
Inorg. Chem. XXXX, XXX, XXX−XXX

Table 1. Atomic Positions, Bond Lengths (Å), and Results of Bond Valence Sum (BVS) Calculations in $DyCrWO_6$ Obtained from the Combined Rietveld Refinement of Room Temperature Synchrotron X-ray (λ = 0.3171 Å) and Neutron (λ = 1.594 Å) Diffraction Data[a]

atom	Wyckoff position	x	y	z	B_{iso} (Å^2)	occupancy
Dy	4a	0.0430(1)	0.4542(3)	1/4	0.48(2)	1
Cr	4a	0.1340(4)	0.9513(10)	0.9962(17)	0.11(7)	1
W	4a	0.3531(1)	0.4443(3)	0.0044(6)	0.44(2)	1
O1	4a	0.9773(13)	0.7688(29)	0.0465(24)	0.67(31)	1
O2	4a	0.5273(13)	0.2588(30)	0.9647(26)	0.99(35)	1
O3	4a	0.2053(12)	0.6161(26)	0.0607(23)	0.75(27)	1
O4	4a	0.2822(12)	0.1263(25)	0.9349(21)	0.47(24)	1
O5	4a	0.1429(5)	0.0585(13)	0.2473(35)	0.66(9)	1
O6	4a	0.1202(6)	0.8340(12)	0.7492(40)	0.75(10)	1

cation	O1	O2	O3	O4	O5	O6
Dy	2.32(1)	2.36(2)	2.39(1)	2.50(1)	2.32(1)	2.32(1)
	2.47(1)	2.37(0)				
Cr	1.98(1)	1.91(2)	1.96(2)	1.90(1)	1.92(0)	1.92(0)
W	2.03(1)	2.14(1)	1.88(1)	1.89(1)	1.98 (0)	1.90(0)

Dy_{BVS}	2.90(4)	W_{BVS}	5.34(12)
Cr_{BVS}	3.42(8)		

[a]Space group $Pna2_1$; a = 10.87855(2) Å, b = 5.18328(1) Å, c = 7.32152(2) Å, $\alpha = \beta = \gamma = 90°$, V = 412.836(1) Å^3; χ^2 = 1.40 (for neutron), χ^2 = 3.92 (for synchrotron); Bragg R factor = 5.35%, R_f factor = 3.56% (for neutron); Bragg R factor = 7.01%, R_f factor = 6.68% (for synchrotron). The origin is floating along the z axis in this space group. We have selected the fixed coordinate z = $^1/_4$ of the Dy atom to fix the origin.

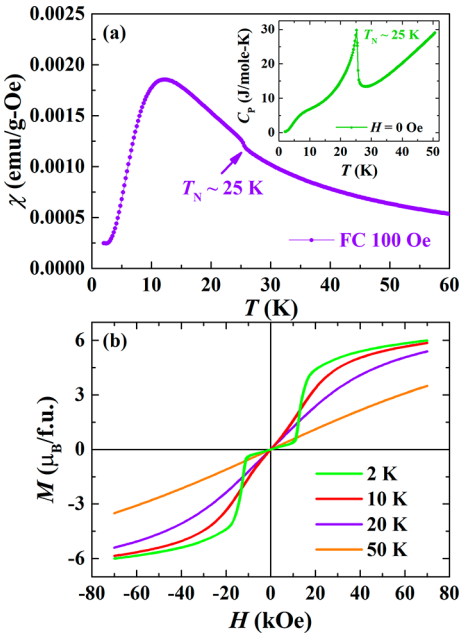

Figure 3. (a) Temperature variation of the FC magnetic susceptibility $\chi(T)$ measured under a magnetic field of 100 Oe. The inset shows the temperature-dependent heat capacity $C_P(T)$. (b) Magnetic-field-dependent magnetization $M(H)$ measured at different temperatures.

moment (μ_{cal} = 11.3 μ_B/fu). The Curie–Weiss temperature is found to be θ_{CW} = −3.5 K. The negative sign of θ_{CW} indicates that the dominant magnetic interaction is antiferromagnetic; however, the absolute value of θ_{CW} is less than T_N. Magnetic-field-dependent magnetization $M(H)$ data measured at different temperatures are shown in Figure 3b. At 2 K, a magnetic-field-induced metamagnetic phase transition is observed, which is certainly due to a field-induced change in the magnetic structure of Dy^{3+} spins, provoking a net macroscopic magnetization. With increasing temperature (as shown at 10 and 20 K), the metamagnetic transition disappears and the behavior is consistent with the global antiferromagnetic nature of both the Cr^{3+} and Dy^{3+} spins.

Temperature-dependent FC susceptibility $\chi(T)$ data measured under different magnetic fields are shown in Figure 4.

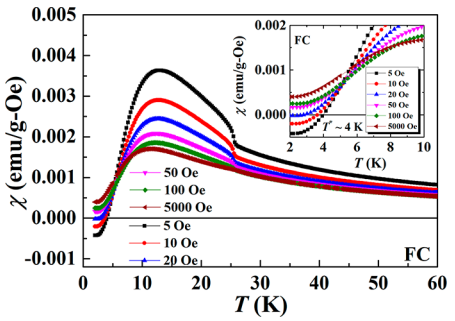

Figure 4. Temperature-dependent FC susceptibility $\chi(T)$ measured with different positive magnetic fields. The inset shows a magnified view of $\chi(T)$ at low temperature.

Upon cooling, $\chi(T)$ increases below T_N initially and then it decreases below 10 K. Upon further cooling, surprisingly, the magnetization becomes negative below a compensation temperature T^* ~ 4 K, when it was measured under a low magnetic field of +5 Oe. With increasing magnetic field, the compensation temperature T^* shifts to lower temperature (inset of Figure 4) and the magnetization becomes positive above a magnetic field of H > 20 Oe. Similar but opposite behavior of $\chi(T)$ is observed in the presence of negative magnetic fields (shown in Figure S2). The magnetization reversal is qualitatively explained in terms of the presence of antiparallel coupling of distinct kinds of magnetic moments (ferrimagnetism). This is not, obviously, the case for $DyCrWO_6$, which shows a strongly noncollinear magnetic

DOI: 10.1021/acs.inorgchem.8b02023
Inorg. Chem. XXXX, XXX, XXX−XXX

structure. In this case, this qualitative explanation may be kept considering only particular components of the magnetic moments. Our experimental data demonstrate that the temperature-induced magnetization reversal at low temperatures may result from antiparallel coupling of some components of the Dy^{3+} and Cr^{3+} moments that may be uncompensated under a small applied magnetic field. The behavior of the complex magnetic structure of $DyCrWO_6$ (Figure 9) under a weak field is very difficult to determine even with single crystals because the change in the magnetic structure should be very small. A similar magnetization reversal is reported, for example, in $SmFeO_3$[16,17] and in some $RCrO_3$ (R = rare-earth element).[18−21]

For further confirmation of magnetization reversal, an isothermal magnetization switching experiment was performed at 2 K. In this measurement, the sample was cooled to 2 K under a magnetic field of +5 Oe, and then the magnetization was measured with time by oscillating the magnetic field between +5 and +17 Oe with a rate of 2 Oe/s. The result of the magnetization switching experiment is shown in Figure 5.

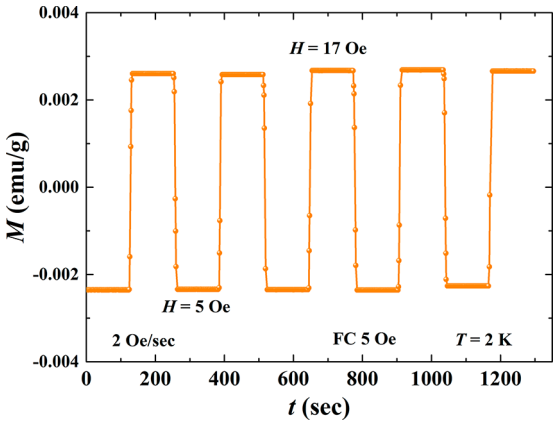

Figure 5. Magnetization switching at 2 K under an oscillating magnetic field between +5 and +17 Oe.

It is clear from the figure that the magnetization can be switched from negative to positive value by varying the field from +5 to +17 Oe. Note that, in ferromagnetic materials, only switching the polarity of the magnetic field can reverse the magnetization. In the present case, varying the magnetic field in the same direction can reverse the magnetization.

Because the applied magnetic field changes the magnetic state at low temperatures, we have explored the magnetocaloric effect. The entropy of a magnetic material changes while it is placed in a changing magnetic field that causes a change in the temperature of the material under adiabatic conditions, known as the magnetocaloric effect. In order to estimate the change in the magnetic entropy in the present compound, the magnetic-field-dependent magnetization at several temperatures was measured. The change in entropy is calculated using the following equation:

$$\Delta S(T, H) = \int_0^H \left(\frac{\partial M}{\partial T}\right)_H \mathrm{d}H$$

The entropy change (ΔS) under various magnetic fields is shown in Figure 6. A large value of the change in entropy is observed at low temperature with a maximum value of ~6 J/kg·K around 12 K under a magnetic field of 70 kOe, which is quite high in the oxide systems. A clear anomaly in ΔS is

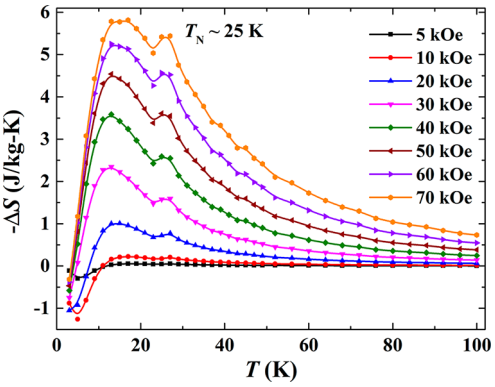

Figure 6. Temperature-dependent entropy changes ΔS under different magnetic fields.

observed around T_N. Upon cooling, ΔS changes its sign at a further lower temperature. This behavior is related to the metamagnetic behavior observed in the magnetization measurements. Similar values and nature of $\Delta S(T)$ at 70 kOe are obtained from the heat capacity data (shown in Figure S3).

The temperature-dependent dielectric constant $\varepsilon_r(T)$ and dielectric loss measured with various frequencies are shown in parts a and b of Figure 7, respectively. Below 200 K, $\varepsilon_r(T)$ is

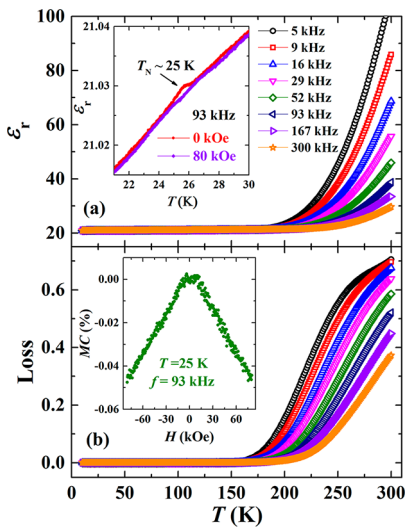

Figure 7. (a) Temperature-dependent dielectric constant $\varepsilon_r(T)$ and (b) loss measured with various frequencies. The temperature-dependent ε_r (T) at 93 kHz measured under 0 and 80 kOe is shown in the inset of part a. The inset of part b shows the magnetocapacitance at T_N ~ 25 K.

almost independent of the temperature and frequency down to the lowest temperature, where the dielectric loss is very small and also independent of the temperature and frequency. Above 200 K, $\varepsilon_r(T)$ increases with increasing temperature, which could be due to the increase in the conductivity of the sample. This is consistent with the increase of dielectric loss with increasing temperature. Interestingly, an anomaly in $\varepsilon_r(T)$ is observed at the antiferromagnetic ordering temperature T_N ~ 25 K (as shown for 93 kHz in the inset of Figure 7a), which does not shift with varying frequencies, indicating the presence of the magnetodielectric effect. However, the magnitude of the dielectric anomaly is very weak compared to the $RFeWO_6$

DOI: 10.1021/acs.inorgchem.8b02023
Inorg. Chem. XXXX, XXX, XXX−XXX

systems.[10] Further, no anomaly is found in the dielectric loss data at T_N. Under a magnetic field of 80 kOe, the anomaly in $\varepsilon_r(T)$ is completely suppressed. The magnetocapacitance measured at $T_N \sim 25$ K shows the presence of a small but finite value (inset of Figure 7b). To find out whether the dielectric anomaly at T_N is associated with any change in the electric polarization, pyroelectric current measurements were carried out across the antiferromagnetic ordering temperature, but we could not detect any pyroelectric current. This indicates that either the electric polarization is very small, which is beyond our instrumental detection limit, or the magnetic structure is different from those of $RFeWO_6$ compounds, which does not induce polarization at T_N.

In order to understand the absence of electric polarization at T_N in $DyCrWO_6$, we determined the magnetic structure by a combination of symmetry analysis and simulated annealing. We also compare and contrast the magnetic structures of the Fe and Cr compounds and suggest possible reasons for not observing ferroelectric polarization in the latter compounds. The neutron data at 3.5 K showed additional Bragg peaks, which could be indexed with the propagation vector $\mathbf{k} = (0, 0, 0)$. It should be noted that the propagation vector in the case of $DyFeWO_6$ was found to be $\mathbf{k} = (0, {}^1/_2, {}^1/_2)$. The representation analysis using *BasIreps*[22] for $Pna2_1$ and $\mathbf{k} = (0, 0, 0)$ provides four one-dimensional irreducible representations, corresponding to the Shubnikov groups: Γ_1: $Pna2_1$, Γ_2: $Pn'a'2_1$, Γ_3: $Pn'a2'_1$, Γ_4: $Pna'2'_1$. These are maximal subgroups of the paramagnetic group $Pna2_11'$, but none of them provide an adequate refinement of the experimental data.

Therefore, we have used simulated annealing by extracting clusters of integrated intensities in $P1$ in order to check whether a solution of higher symmetry was possible. From the nonmaximal subgroups obtained with the Bilbao Crystallographic Server program *k-Subgroupmag*,[23] only the $P112_1$ group was plausible (R factor below 25% in simulated annealing). This group corresponds to mixing of the representations: $\Gamma_1 \oplus \Gamma_2$. This group splits all of the atoms, so instead of the 9 atoms in the asymmetric unit of $Pna2_1$, we have 18 atoms in $P112_1$. Because the refinement of all parameters was not stable, we preferred to treat the nuclear contribution using the $Pna2_1$ group and the magnetic contribution using the $P112_1$ group. However, refinement of the magnetic structure with four atoms, two Dy and two Cr, in the magnetic asymmetric unit (12 free parameters) was also unstable, but we realized that some approximate relations appeared in the components of the two inequivalent split atoms.

Finally, we applied the following additional constraints between the moments of Dy1 and Dy2, as well as Cr1 and Cr2: the magnetic moment of the second atom was obtained from the magnetic moment of the first by putting the same m_x and m_y components and opposite m_z components. With these constraints we reduce the number of parameters to 6 instead of 12; moreover, the values of the moments are automatically the same for both independent sites, and, finally, the refinement was excellent, as shown in Figure 8, where the inset shows the magnified view of the neutron diffraction pattern at low angles. The added constraint is equivalent to the operator $(u, v, -w)$ acting on the magnetic moments, which is associated with the $Pna2_1$ symmetry operator $(x + {}^1/_2, -y + {}^1/_2, z)$ that does not belong to the $P112_1$ magnetic group. We noticed that the obtained value of the magnetic moment of Cr^{3+} ions was a little bit higher than the expected 3 μ_B, so we added a soft

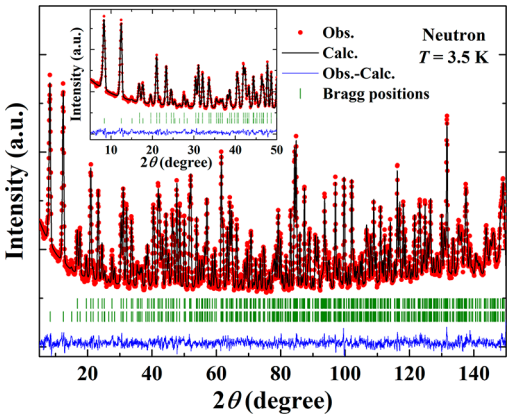

Figure 8. Rietveld refinement of the crystal and magnetic structures of $DyCrWO_6$ at $T = 3.5$ K. The magnetic peaks are those of the second row of tick marks. The inset shows the magnified view of the neutron diffraction data at low angles.

constraint for having a moment of 2.9 μ_B with a σ value of 0.03 μ_B that maintains a reasonable value without changing the quality of the refinement. The details of final crystal and magnetic structures of $DyCrWO_6$ at 3.5 K are given in Tables 2 and 3, respectively. The obtained magnetic structure is displayed in Figure 9.

One can see that the spin configuration of Cr atoms is formed by ferromagnetic layers, (Cr1,Cr2)_1 and (Cr1,Cr2)_2, perpendicular to the c axis, stacked antiferromagnetically along c. The configuration is nearly collinear except for a small tilt in the z component that is zero within the standard deviation. This arrangement of Cr spins is different from that of $DyFeWO_6$, where Fe spins form a strongly noncollinear configuration. In this kind of structure, the transition-metal sublattices interact only through super-superexchange interaction involving at least two O ions, so they are weaker than normal superexchange interactions involving only one O ligand.

The interactions between the Cr and Dy ions, J_{Cr-Dy}, are of superexchange nature, but because of the inner 4f electrons of Dy ions, the overlap should be quite small and these exchange interactions are weaker than the Cr−O−O−Cr interactions. Still weaker are the Dy−O−Dy superexchange interactions that take place through corners of O1 and O2 atoms and edges of O1−O3, O1−O6, and O2−O5. However, it is interesting to note that refinement of the neutron data at intermediate temperatures (15 and 20 K) indicates induced ordering of Dy spins at the Cr-ordering temperature ($T_N = 25$ K) due to the combined effect of the local field due to Cr ordering and the anisotropy of Dy ions.

We have performed calculation of a phase diagram of the first ordered state considering only the Cr sublattices. This mean-field calculation for classical spins is based on ref 24 but using an interaction energy for pairs of spins of the form

$$E_{ij} = -J_{ij} S_i \cdot S_j$$

where the negative sign means that the energy of the pair is minimized for a negative exchange interaction when the spins are antiparallel (antiferromagnetic coupling). The first ordered state (just below T_N) of a magnetic system is given as a function of the $\mathbf{k}$ vector inside or at the surface of the Brillouin zone by the eigenvector corresponding to the lowest

DOI: 10.1021/acs.inorgchem.8b02023
Inorg. Chem. XXXX, XXX, XXX−XXX

Table 2. Crystal Structure of $DyCrWO_6$ Treated in the Space Group $Pna2_1$ at 3.5 K[a]

atom	Wyckoff position	x	y	z	B_{iso} (Å^2)	occupancy
Dy	4a	0.0428(1)	0.4548(2)	1/4	0.26(3)	1
Cr	4a	0.1352(12)	0.9514(42)	0.9965(20)	0.60(6)	1
W	4a	0.3552(9)	0.4498(33)	0.0039(16)	0.60(6)	1
O1	4a	0.9745(12)	0.7708(19)	0.0488(15)	0.46(3)	1
O2	4a	0.5242(11)	0.2571(21)	0.9662(14)	0.46(3)	1
O3	4a	0.2171(7)	0.6170(19)	0.0596(16)	0.46(3)	1
O4	4a	0.2956(7)	0.1265(20)	0.9335(15)	0.46(3)	1
O5	4a	0.1438(3)	0.0580(9)	0.2507(33)	0.46(3)	1
O6	4a	0.1208(4)	0.8345(7)	0.7558(26)	0.46(3)	1
cation	O1	O2	O3	O4	O5	O6
Dy	2.32(1)	2.34(1)	2.50(1)	2.38(1)	2.33(1)	2.33(0)
	2.48(1)	2.36(1)				
Cr	2.02(2)	1.95(2)	2.00(2)	2.02(2)	1.95(3)	1.86(3)
W	1.97(2)	2.11(2)	1.78(1)	1.87(2)	1.93(2)	1.96(2)

Dy_{BVS}	2.91(2)	W_{BVS}	5.90(13)
Cr_{BVS}	3.15(8)		

[a]Space group $Pna2_1$; a = 10.88056(9) Å, b = 5.17746(5) Å, c = 7.31431(6) Å, $\alpha = \beta = \gamma = 90°$, V = 412.042(6) Å^3; χ^2 = 1.98, Bragg R factor = 3.84%, R_f factor = 2.28%. Bond lengths are given in Å.

Table 3. Magnetic Structure of $DyCrWO_6$ at 3.5 K Treated in the Space Group $P112_1$ with Additional Constraints Linking the Independent Sites (R_{Mag} = 4.39%) and a Complete List of Atoms in the Unit Cell and Symmetry Operators of $Pna2_1$ Relating the Different Atom Positions as Well as the Corresponding Magnetic Moments

atom	m_x	m_y	m_z	moment (μ_B)	
Dy1	1.69(19)	−5.90(7)	−4.77(3)	7.77(4)	
Dy2	1.69(19)	−5.90(7)	4.77(3)	7.77(4)	constraint (m_x, m_y, $-m_z$)
Cr1	0.90(29)	2.78(9)	0.03(5)	2.92(3)	
Cr2	0.90(29)	2.78(9)	−0.03(5)	2.92(3)	constraint (m_x, m_y, $-m_z$)

atom	m_x	m_y	m_z		
Dy1_1	1.69(19)	−5.90(7)	−4.77(3)	x, y, z	u, v, w
Dy1_2	−1.69(19)	5.90(7)	−4.77(3)	$-x$, $-y$, $z + {}^1/_2$	$-u$, $-v$, w
Dy2_1	1.69(19)	−5.90(7)	4.77(3)	$x + {}^1/_2$, $-y + {}^1/_2$, z	u, v, $-w$
Dy2_2	−1.69(19)	5.90(7)	4.77(3)	$-x + {}^1/_2$, $y + {}^1/_2$, $z + {}^1/_2$	$-u$, $-v$, $-w$
Cr1_1	0.90(29)	2.78(9)	0.03(5)	x, y, z	u, v, w
Cr1_2	−0.90(29)	−2.78(9)	0.03(5)	$-x$, $-y$, $z + {}^1/_2$	$-u$, $-v$, w
Cr2_1	0.90(29)	2.78(9)	−0.03(5)	$x + {}^1/_2$, $-y + {}^1/_2$, z	u, v, $-w$
Cr2_2	−0.90(29)	−2.78(9)	−0.03(5)	$-x + {}^1/_2$, $y + {}^1/_2$, $z + {}^1/_2$	$-u$, $-v$, $-w$

[a]If we use the notation of Bertaut[26] for magnetic modes G = (+ − + −), C = (+ − − +), A = (+ + − −), and F = (+ + + +) and using the particular numbering of the four atoms in $Pna2_1$ according with the list of operators, we have, for the two magnetic atoms in the asymmetric unit of the paramagnetic group, the same configurations of modes, i.e., (G_x, G_y, A_z).

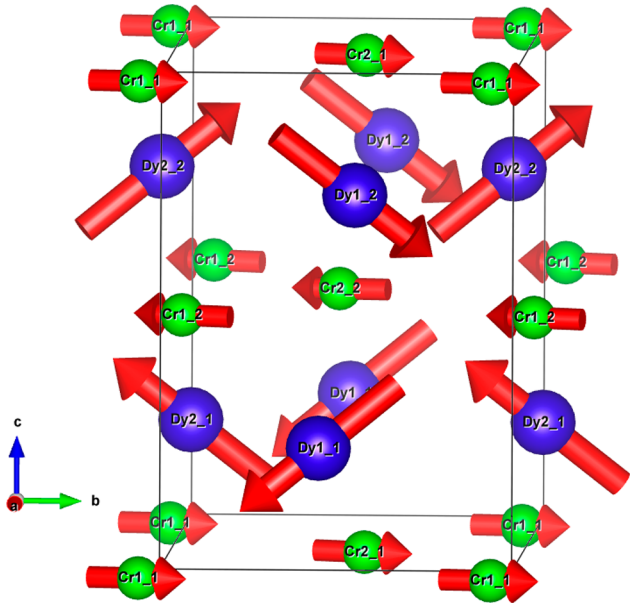

Figure 9. Magnetic structure of $DyCrWO_6$ at T = 3.5 K. The blue atoms are Dy, and the green atoms are Cr. The numbering is as follows: Sy_n (Sy = Dy1, Dy2, Cr1, Cr2; n = 1, 2). The atoms n = 1 and 2 correspond to the symmetry operators (x, y, z) and ($-x$, $-y$, z + ${}^1/_2$) of the $P112_1$ magnetic group.

eigenvalue of the negative Fourier transform of the exchange interaction matrix:

$$\xi_{ij}(k) = -\sum_m J_{ij}(R_m)\, e^{-2\pi i k R_m}$$

where the indices i and j are the numbers of magnetic atoms of a primitive cell and R_m is a lattice translation.

For doing the calculations, we have used the programs *Simbo* and *EnerMag*,[25] considering only three exchange interactions between Cr ions, as detailed in Figure 10a,b. The program *Simbo* provides independent exchange interactions by analyzing the possible superexchange (or super-superexchange) paths between magnetic atoms. The exchange interaction J_1 corresponds to the shortest Cr−Cr distance, and the others

DOI: 10.1021/acs.inorgchem.8b02023
Inorg. Chem. XXXX, XXX, XXX−XXX

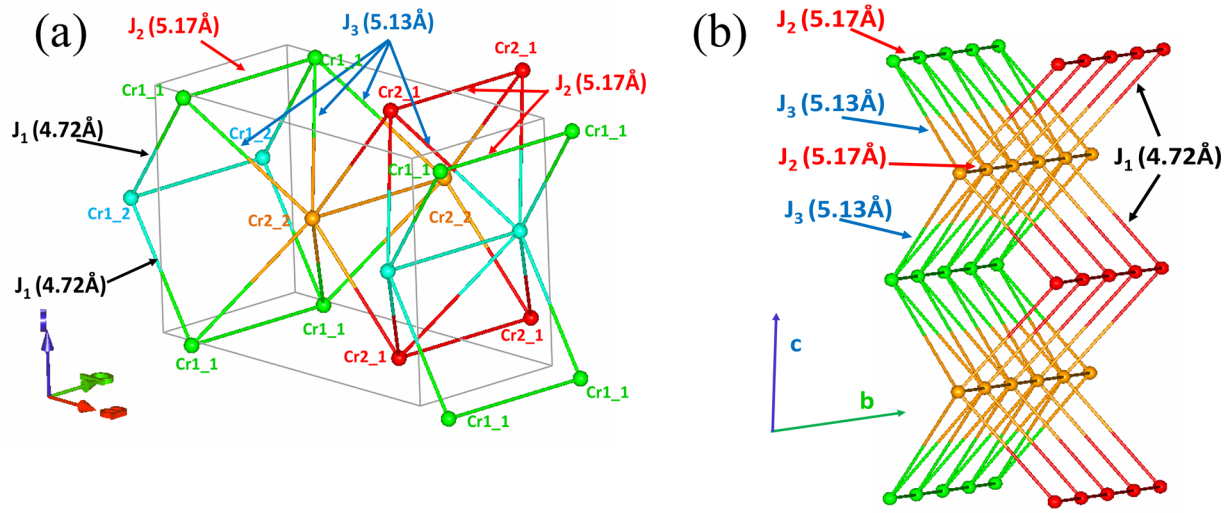

Figure 10. (a) Topology of the isotropic exchange interactions between Cr ions in $DyCrWO_6$. All of the connected atoms are below a distance of 5.3 Å between each other and correspond to super-superexchange interactions involving Cr−O−O−Cr paths. The distances between Cr atoms are indicated in parentheses. (b) Details of the puckered triangular and rectangular sheets running along the *b* and *c* axes, in which we show the three independent super-superexchange interactions. It is expected that all of the exchange interactions are negative because in octahedral coordination the electronic configuration is t_{2g}^3 for Cr^{3+} ions. So, a certain degree of frustration in the triangular sheets is expected.

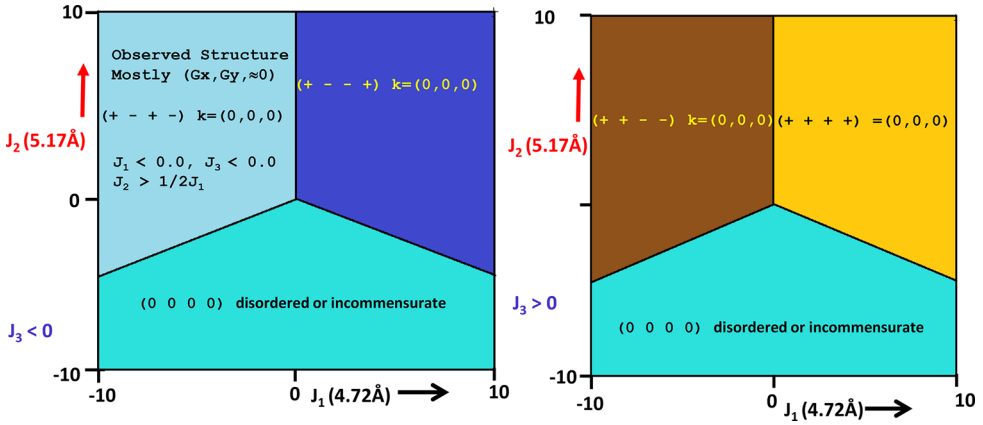

Figure 11. Phase diagram of the Cr sublattices of $DyCrWO_6$ considering three isotropic exchange interactions, as detailed in previous figures. The different colors correspond to different kinds of magnetic structures. The sequence of the signs corresponds to the moments along an arbitrary direction (a global rotation does not change the energy because of the isotropic character of exchanges considered here). We have neglected the boundaries with $J_i = 0$, where partial orders appear. The observed structure corresponds to $\mathbf{k} = (0, 0, 0)$ and the sequence G(+ − + −).

are numbered arbitrarily. The program *EnerMag* performs diagonalization of the matrix $\xi_{ij}(k)$ as a function of the exchange interactions and **k**. For details, refer to the appendix of ref 25.

We have varied the three exchange interactions between −10 and +10 in arbitrary units (only the relative values are relevant) and calculated the first ordered state for each triplet of exchanges. The results are summarized in Figure 11. One can see that the observed magnetic structure for the Cr sublattices corresponds to the conditions $J_1 < 0.0$, $J_3 < 0.0$, and $J_2 > {}^1/_2 J_1$. This means that the observed magnetic structure is compatible with a set of negative (antiferromagnetic) exchange interactions provided that $J_2 > {}^1/_2 J_1$. Notice that, in the regions where $J_2 > {}^1/_2 J_1$ and $J_3 < 0$, no magnetic order is established or incommensurate magnetic structures may appear (the details of the ground state cannot be determined with the present method), reflecting the frustration in the puckered triangular sheets.

The ordering of the Dy sublattices is determined mostly by the single-ion anisotropy of Dy^{3+} ions and the exchange interactions J_{Cr-Dy}. Notice that, except for the propagation vector, the arrangement of the Dy moments is quite similar to that observed in the case of the $DyFeWO_6$ compound. The single-ion anisotropy of Dy is so as to make Dy moment to orient nearly along one O atom and the opposite edge of the coordination polyhedron (Figure S4). The strong non-collinearity of the Fe moments in the magnetic structure of $DyFeWO_6$ means that the exchange interactions J_{Fe-Dy} are much stronger than J_{Cr-Dy} probably because of the involvement of e_g^2 electrons and the magnetic moments of Fe have a tendency to reorient according to the local direction of the Dy moments. The collinearity observed in the Cr sublattices of $DyCrWO_6$ may be the reason why we are unable to detect an electric polarization, at variance with the case of $DyFeWO_6$. However, it requires further study, for example, the magnetic structure of multiferroic $YFeWO_6$, to confirm the

DOI: 10.1021/acs.inorgchem.8b02023
Inorg. Chem. XXXX, XXX, XXX−XXX

origin and role of noncollinearity in inducing electric polarization in these compounds.

IV. CONCLUSIONS

In conclusion, we have shown that the compound $DyCrWO_6$ crystallizes in the ordered aeschynite-type polar structure ($Pna2_1$). It exhibits a long-range antiferromagnetic ordering of Cr sublattices and induced ordering of Dy sublattices below $T_N \sim 25$ K. The obtained magnetic structure consisted of a collinear arrangement of Cr^{3+} moments and a noncollinear arrangement of Dy^{3+} moments. At low temperature, magnetization reversal occurs, which is caused by the competition between the Dy^{3+} and Cr^{3+} moments. A large value of entropy change is observed at low temperature under an applied magnetic field. This may be related to the metamagnetic behavior of the Dy^{3+}-spin configuration. A weak dielectric anomaly and magnetocapacitance are observed around T_N; however, electric polarization is not found, which could be due to the collinear arrangement of Cr spins compared to that of $RFeWO_6$, where both Fe and Dy sublattices exhibit noncollinear arrangement.

■ ASSOCIATED CONTENT

Supporting Information

The Supporting Information is available free of charge on the ACS Publications website at DOI: 10.1021/acs.inorgchem.8b02023.

Additional results including a Curie−Weiss fit of magnetic susceptibility, magnetization reversal under opposite magnetic fields, a comparison of the entropy changes from heat capacity and magnetization data, orientation of the Dy moment with respect to its coordination polyhedron in $DyCrWO_6$ and $DyFeWO_6$, and magnetic moments at different temperatures (PDF)

Accession Codes

CCDC 1856504 contains the supplementary crystallographic data for this paper. These data can be obtained free of charge via www.ccdc.cam.ac.uk/data_request/cif, or by emailing data_request@ccdc.cam.ac.uk, or by contacting The Cambridge Crystallographic Data Centre, 12 Union Road, Cambridge CB2 1EZ, UK; fax: +44 1223 336033.

■ AUTHOR INFORMATION

Corresponding Author

*E-mail: sundaresan@jnacsr.ac.in.

ORCID

A. Sundaresan: 0000-0002-1613-3030

Notes

The authors declare no competing financial interest.

■ ACKNOWLEDGMENTS

S.G. and A.S. acknowledge the Department of Science and Technology, India (Grant SR/NM/Z-07/2015), for financial support in performing synchrotron X-ray diffraction experiments (Proposal 2015091465) at ALBA, Barcelona, Spain, and Jawaharlal Nehru Centre for Advanced Scientific Research for managing the project. S.G. and A.S. thank the International Centre for Materials Science and Sheikh Saqr Laboratory at Jawaharlal Nehru Centre for Advanced Scientific Research for providing various experimental facilities. S.G. acknowledges Jawaharlal Nehru Centre for Advanced Scientific Research for providing a research associate fellowship (JNC/T1196).

■ REFERENCES

(1) Choi, Y.; Yi, H.; Lee, S.; Huang, Q.; Kiryukhin, V.; Cheong, S.-W. Ferroelectricity in an Ising chain magnet. *Phys. Rev. Lett.* **2008**, *100*, 047601.

(2) Kimura, T.; Goto, T.; Shintani, H.; Ishizaka, K.; Arima, T.; Tokura, Y. Magnetic control of ferroelectric polarization. *Nature* **2003**, *426*, 55−58.

(3) Yamasaki, Y.; Miyasaka, S.; Kaneko, Y.; He, J.-P.; Arima, T.; Tokura, Y. Magnetic reversal of the ferroelectric polarization in a multiferroic spinel oxide. *Phys. Rev. Lett.* **2006**, *96*, 207204.

(4) Tokura, Y.; Seki, S.; Nagaosa, N. Multiferroics of spin origin. *Rep. Prog. Phys.* **2014**, *77*, 076501.

(5) Oh, Y. S.; Artyukhin, S.; Yang, J. J.; Zapf, V.; Kim, J. W.; Vanderbilt, D.; Cheong, S.-W. Non-hysteretic colossal magnetoelectricity in a collinear antiferromagnet. *Nat. Commun.* **2014**, *5*. DOI: 10.1038/ncomms4201

(6) Wang, Y.; Pascut, G. L.; Gao, B.; Tyson, T. A.; Haule, K.; Kiryukhin, V.; Cheong, S.-W. Unveiling hidden ferrimagnetism and giant magnetoelectricity in polar magnet $Fe_2Mo_3O_8$. *Sci. Rep.* **2015**, *5*. DOI: 10.1038/srep12268

(7) Kurumaji, T.; Ishiwata, S.; Tokura, Y. Doping-Tunable Ferrimagnetic Phase with Large Linear Magnetoelectric Effect in a Polar Magnet $Fe_2Mo_3O_8$. *Phys. Rev. X* **2015**, *5*, 031034.

(8) Kurumaji, T.; Ishiwata, S.; Tokura, Y. Diagonal magnetoelectric susceptibility and effect of Fe doping in the polar ferrimagnet $Mn_2Mo_3O_8$. *Phys. Rev. B: Condens. Matter Mater. Phys.* **2017**, *95*, 045142.

(9) Caignaert, V.; Maignan, A.; Singh, K.; Simon, C.; Pralong, V.; Raveau, B.; Mitchell, J. F.; Zheng, H.; Huq, A.; Chapon, L. Gigantic magnetic-field-induced polarization and magnetoelectric coupling in a ferrimagnetic oxide $CaBaCo_4O_7$. *Phys. Rev. B: Condens. Matter Mater. Phys.* **2013**, *88*, 174403.

(10) Ghara, S.; Suard, E.; Fauth, F.; Tran, T. T.; Halasyamani, P. S.; Iyo, A.; Rodríguez-Carvajal, J.; Sundaresan, A. Ordered aeschynite-type polar magnets $RFeWO_6$ (R= Dy, Eu, Tb, and Y): A new family of type-II multiferroics. *Phys. Rev. B: Condens. Matter Mater. Phys.* **2017**, *95*, 224416.

(11) Salmon, R.; Baudry, H.; Grannec, J.; Le Flem, G. Sur de nouvelles séries de composés du tungstène+ IV de type aeschynite. *Rev. Chim. Miner.* **1974**, *11*, 71−79.

(12) Kim, S. W.; Emge, T. J.; Deng, Z.; Uppuluri, R.; Collins, L.; Lapidus, S. H.; Segre, C. U.; Croft, M.; Jin, C.; Gopalan, V.; Kalinin, S. V.; Greenblatt, M. $YCrWO_6$: Polar and Magnetic Oxide with $CaTa_2O_6$-Related Structure. *Chem. Mater.* **2018**, *30*, 1045−1054.

(13) Fauth, F.; Boer, R.; Gil-Ortiz, F.; Popescu, C.; Vallcorba, O.; Peral, I.; Fullà, D.; Benach, J.; Juanhuix, J. The crystallography stations at the Alba synchrotron. *Eur. Phys. J. Plus* **2015**, *130*, 160.

(14) Fauth, F.; Peral, I.; Popescu, C.; Knapp, M. The new material science powder diffraction beamline at ALBA synchrotron. *Powder Diffr.* **2013**, *28*, S360−S370.

(15) Rietveld, H. A profile refinement method for nuclear and magnetic structures. *J. Appl. Crystallogr.* **1969**, *2*, 65−71.

(16) Lee, J.-H.; Jeong, Y. K.; Park, J. H.; Oak, M.-A.; Jang, H. M.; Son, J. Y.; Scott, J. F. Spin-Canting-Induced Improper Ferroelectricity and Spontaneous Magnetization Reversal in $SmFeO_3$. *Phys. Rev. Lett.* **2011**, *107*, 117201.

(17) Jeong, Y. K.; Lee, J.-H.; Ahn, S.-J.; Jang, H. M. Temperature-induced magnetization reversal and ultra-fast magnetic switch at low field in $SmFeO_3$. *Solid State Commun.* **2012**, *152*, 1112−1115.

(18) Yoshii, K. Magnetization reversal in $TmCrO_3$. *Mater. Res. Bull.* **2012**, *47*, 3243−3248.

(19) Cao, Y.; Cao, S.; Ren, W.; Feng, Z.; Yuan, S.; Kang, B.; Lu, B.; Zhang, J. Magnetization switching of rare earth orthochromite $CeCrO_3$. *Appl. Phys. Lett.* **2014**, *104*, 232405.

DOI: 10.1021/acs.inorgchem.8b02023
Inorg. Chem. XXXX, XXX, XXX−XXX

(20) Wang, L.; Wang, S.; Zhang, X.; Zhang, L.; Yao, R.; Rao, G. Reversals of magnetization and exchange-bias in perovskite chromite $YbCrO_3$. *J. Alloys Compd.* **2016**, *662*, 268−271.
(21) Zhao, H. J.; Íñiguez, J.; Chen, X. M.; Bellaiche, L. Origin of the magnetization and compensation temperature in rare-earth orthoferrites and orthochromates. *Phys. Rev. B: Condens. Matter Mater. Phys.* **2016**, *93*, 014417.
(22) Rodriguez-Carvajal, J. *BasIreps: a Program for Calculating Irreducible Representations of Little Groups and Basis Functions of Polar and Axial Vector Properties* (unpublished, 2004). Program distributed within the *FullProf* Suite.
(23) Perez-Mato, J.; Gallego, S.; Elcoro, L.; Tasci, E.; Aroyo, M. Symmetry conditions for type II multiferroicity in commensurate magnetic structures. *J. Phys.: Condens. Matter* **2016**, *28*, 286001.
(24) Freiser, M. J. Thermal variation of the pitch of helical spin configurations. *Phys. Rev.* **1961**, *123*, 2003.
(25) El Khayati, N.; Cherkaoui El Moursli, R.; Rodríguez-Carvajal, J.; André, G.; Blanchard, N.; Bourée, F.; Collin, G.; Roisnel, T. Crystal and magnetic structures of the oxyphosphates $MFePO_5$ (M= Fe, Co, Ni, Cu). Analysis of the magnetic ground state in terms of superexchange interactions. *Eur. Phys. J. B* **2001**, *22*, 429−442. The programs *Simbo* and *EnerMag* are distributed within the *MagPack* package, which can be obtained at https://forge.epn-campus.eu/projects/crysfml/files for the Windows and Linux platforms.
(26) Bertaut, E. F. Representation analysis of magnetic structures. *Acta Crystallogr., Sect. A: Cryst. Phys., Diffr., Theor. Gen. Crystallogr.* **1968**, *24*, 217.

DOI: 10.1021/acs.inorgchem.8b02023
Inorg. Chem. XXXX, XXX, XXX−XXX